Numerical Computation of Non-linear Convection Flow of Micro-polar Fluids over Non-Isothermal Cylinder

wubshet ibrahim[1] and Chaluma Zemedu[1]

[1]Ambo University

March 07, 2024

Abstract

The aim of this article is to analyze the impacts of Eckert, surface temperature and heat flux on two boundary layer flow of non-linear convection flow of micro-polar fluid past non-isothermal cylinder. The mathematical modeling for the flow problem has been created with suitable similarity transformation and dimensionless variable. The main nonlinear boundary value problems were reduced into mixed high order non-linear ordinary differential equations. The equations were solved using the method bvp4c from matlab software for numerous quantities of main constraints. The impacts of constraints on velocities, surface temperature and heat flux are examined and displayed through the graphs and tables. The convergence test has been maintained; for number of spots greater than apposite mesh number of spots, the precision is not affected. Moreover, a comparison with previous paper reachable in the literature has been reported and an excellent agreement is obtained. The acquiring shows that enhancing in the values of surface temperature and heat flux constraints (F, H) is to improve thermal diffusion that improve temperature distributions q(h);h(h).

Numerical computation of Non-linear Convection Flow of Micro-polar Fluids over Non-Isothermal Cylinder

Chaluma Zemedu and Wubshet Ibrahim *
Department of Mathematics, Ambo University,Ambo, Ethiopia

May 5, 2021

Abstract

The aim of this article is to analysis the impacts of Eckert, surface temperature and heat flux on edge sheet flow of nonlinear convection stream of micro-polar fluid past non-isothermal cylinder. The mathematical modeling for the stream trouble has been created by suitable likeness change with dimensionless variables. The main nonlinear limit importance problems were simplified into mixed high regulate nonlinear ordinary degree of difference equations. The equations were calculated by using the idea bvp4c from matlab software for numerous amount of main constraints. Impacts of constraints on velocities, surface temperature and heat flux are examined and displayed from side to side the diagrams and charts. The junction examination has been sustained; For digit of spots superior than apposite mesh digit of spots, the exactitude is not affected. More to the point, a comparison with previous study reachable in the literature has been reported and an excellent concurrence is got. The acquiring show that enhancing in the values of surface temperature and heat flux constraints (F, H) is to improve thermal diffusion that improve temperature distributions $\theta(\eta), h(\eta)$. .

Keywords*: Nonlinear convection flow; Micro-polar fluid; Non-Isothermal cylinder.*

*Corresponding author,E-mail: wubshetib@yahoo.com, Tel +251911892494

Nomenclature

a	Momentum jump factor (m^{-1})	q_w	heat flux (Wm^{-2}
b	Radius of cylinder,(m)	T	temperature of the fluid (K)
C_f,	skin friction coefficient	T_w	wall temperature (K)
c_p	specific heat ($JKg^{-1}K^{-1}$)	T_∞	ambient temperature(K)
c	thermal jump factor (m^{-1})	u, v	velocity elements (ms^{-1})
d	Thermal non linear convection parameter	x, y	cartesian coordinates (m)
Ec	Eckert number	Greeks	
F, H	Non-isothermal parameter (power index)	α	Dimensionless stream wise coordinate
Gr	Thermal Grashof number	η	dimensionless similarity variable
G2	Micro rotation slip parameter	θ	dimensionless temperature
G1	Velocity slip parameter	μ	coeff. of dynamic viscosity(Pas)
G3	temperature slip arameter	κ	vortex viscosity coefficient(Pas)
G4	heat flux slip parameter	ν	kinematic viscosity coeff.
h	dimensionless heat flux	ψ	stream functions(m^2s^{-1})
j	Micro inertia density	ρ	fluid density(Kgm^{-3})
K	thermal conductivity ($Wm^{-1}K^{-1}$)	φ	spin -gradient viscosity(m^2s^{-1})
L	dimensionless micro rotation velocity	τ_w	surface shear stress(pa)
M	Micro rotation at surface	λ	microrotation constraint
m_w	Wall couple stress	Subscripts	
N	Constants	∞	states at the free stream
N_t	Thermal volumetric expansion coeffs.	w	state at the wall
Nu	local Nusselt number		
p	dimensionless stream function		
Pr	Prandtl number		

1 Introduction

The study of heat shift has drawn some researchers as result of its appeal to some technological, various engineering and manufacturing growth for example glass making, paper industrialized , the drawing of a polymer sheet, the cooling of metallic plate in bath etc. Pabst [1] has discussed the physical importance of material constraint and the decrement of their number because of symmetry. Moreover, the flow parts in the occurrence of a micro-polar fluid are, indicating a declining behaviour in the flow compared to the velocity components Calmelet and Majumdar [2]. The micro-polar constraints possess a low consequence on start of convection inside holey medium; Enlarging the combining number in micro-polar fluid slows down the flow velocity and increases the angular velocity as presented by Reena and Rena et al.[3] and Gajjela et al.[4].

Machireddy[5] and Shah et al. [6] have reported that the increasing behaviour of transient, radial and tangential velocities are performed with Grashoff number and rotation constraint.

The enhancing behavior of thermal field performed with improve the magnitudes of Eckert number, and thermal relaxation time constraint while the reduction character of it functioned as explained by Reddy et al.([7]-[8]) and Sherzad et al.[9]. Salleh as well as Nazar [10] have studied the combined convection edge sheet stream beginning solid sphere with thermal radiation impact and Newtonian roasting in MHD flow micropolar fluid. Wubshet and Shanker [11] have informed the manipulates of magnetic area and thermal radiation on nanofluid past non-isothermal ball along extending layer by non-isothermal wall temperature in addition to

non-isothermal thermal fluctuation. Recently, Wubshet and Chaluma ([12], [13],[14]) have been investigated that increasing in thermal nonlinear convection exhibits the enhancing feature on Nusselt number, skin friction coefficient, velocity fields close the outside of sphere, disk and cylinder while it shows the decreasing behaviour on thermal field. This effect happen due to higher density of the fluid which relates to lower the momentum diffusion and higher thermal diffusion close wall of sphere, disk with cylinder

All the above quoted papers have been presenting the current past a flat surface, isothermal sphere,disk, cylinder. However, we look at the nonlinear free convection run of micropolar fluid onwards a nonisothermal cylinder within the existence of Eckert number, non-isothermal indexes, the microinertia for each unit side, using method bvp4c from matlab. The affects of physical constraints on fluid velocity,angular, heat were presented and revealed in diagrams and charts as well.

2 Mathematical Formulation

Take into consideration a two measurement independent of time boundary layer flow of a viscous micro-polar fluid past a non-isothermal cylinder with constant radius b. Presume a non-isothermal surface temperature $T_w(=T_\infty+\triangle T)$ of cylinder is presumed hotter than at far temperature of the fluid. The temperature at far is T_∞. The coordinate x as well as y are selected such that x events the distance toward the circumference of the cylinder from the lower point and y events the distance usual to the wall of the cylinder along radial as revealed in the Fig. 1.

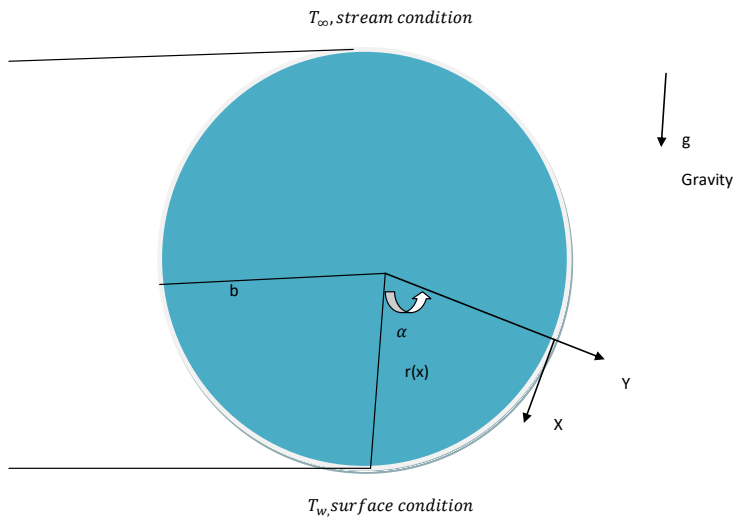

Fig. 1 – Physical and coordinates system

Subsequently, Amanulla. *et al.*[15] the degree of difference equations leading this problems are prearranged as:

$$\frac{\partial(ur)}{\partial x}+\frac{\partial(vr)}{\partial y}=0 \tag{1}$$

$$u\frac{\partial u}{\partial x}+v\frac{\partial u}{\partial y}=(\nu+\frac{\kappa}{\rho})\frac{\partial^2 u}{\partial y^2}+\frac{\kappa}{\rho}\frac{\partial M}{\partial y}+(g(N(T-T_\infty)+N_t(T-T_\infty)^2))\sin(\frac{x}{b}) \tag{2}$$

$$u\frac{\partial M}{\partial x}+v\frac{\partial M}{\partial y}=\frac{\varphi}{\rho j}\frac{\partial^2 M}{\partial y^2}-\frac{\kappa}{\rho j}(2M+\frac{\partial u}{\partial y}) \tag{3}$$

$$u\frac{\partial T}{\partial x}+v\frac{\partial T}{\partial y}=\frac{\kappa}{\rho c_p}\frac{\partial^2 T}{\partial y^2}+\frac{\nu}{c_p}(\frac{\partial u}{\partial y})^2 \tag{4}$$

by means of limit states

$$u=a\frac{\partial u}{\partial y}, u=a\frac{\partial u}{\partial x}, v=0,$$

$$M=-\lambda\frac{\partial u}{\partial y}, M=-\lambda\frac{\partial M}{\partial x}, ony=0 \tag{5}$$

$$u\rightarrow u_\infty, M\rightarrow 0, asy\rightarrow\infty. \tag{6}$$

The thermal limit states are:

1. The arranged wall temperature (AST)

$$T=T_w+c\frac{\partial T}{\partial y}=T_\infty+\frac{x^F}{b}+c\frac{\partial T}{\partial y}, T=T_w+c\frac{\partial T}{\partial x}, \text{ on y=0.}$$

$$T\rightarrow T_\infty, asy\rightarrow\infty. \tag{7}$$

2. The arranged heat flux(AHF)

$$-K\frac{\partial T}{\partial y}=q_w=\frac{x^H}{b}+c\frac{\partial T}{\partial y}, -K\frac{\partial T}{\partial y}=\frac{x^H}{b}+c\frac{\partial T}{\partial x}, \text{ on y=0.}$$

$$T\rightarrow T_\infty, asy\rightarrow\infty. \tag{8}$$

Here are u and v, the elements of velocity in the x as wall as y axes correspondingly, a and c stand for velocity and thermal slip factors, respectively. M is the part of angular velocity normal to the xy flat surface. λ denotes a uniform that lies between 0 and 1. When $\lambda=0$, the intensity of particles are thicken which the microelements in the close of the wall are unable to revolve, when $\lambda=\frac{1}{2}$, the anti-symmetric element of the stress tensor is departure which represents for puny strenth. The case $\lambda=1$ used for developing the turbulent limit layer flows. μ, ρ, $\nu=\frac{\mu}{\rho}$, c_p ,$j=\frac{b^2}{\sqrt{Gr}}$, $\varphi=(\mu+\frac{\kappa}{2})j$,κ,T, K and $T_w(=T_\infty+\triangle T)$ are the coefficient of fluid viscosity, the density, kinematic viscosity, specific heat, micro inertia for each unit size, spin gradient, vortex viscosity, temperature, conductivity of the fluid, transformable temperature on surface, here, $\triangle T$ is constant which gives the rate of growth of temperature alongside the surface and T_∞, g stand for the uniform temperature of the free stream, g represents for the gravity,$\frac{\nabla\rho}{\rho}(=N(T-T_\infty)+N_t(T-T_\infty)^2$, N is stable, N_t is the stable coefficient of thermal volumetric growth. Here the relation will be non-linear density temperature (NDT) change. Let $r(x)=b\sin(\frac{x}{b})$ be the radial remoteness from the symmetrical axis to the outside of the sphere.

From Amanulla. *et al.*[15] the dimensionless changes are:

$\alpha=\frac{x}{b}$, $\eta=\frac{(Gr)^{\frac{1}{4}}}{b}y$, $r=\frac{r*}{b}$, $p=\frac{\psi}{\nu\alpha(Gr)^{\frac{1}{4}}}$,

$$L=\frac{b^2}{\nu\alpha(Gr)^{\frac{3}{4}}}M \tag{9}$$

On behalf of thermal limit states, we take into account non-dimensional measures as next:

(a) On behalf of arranged wall hotness, F is the surface hotness stricture, T_w is the hotness at the wall and b is unchangeable. The dimensionless hotness in AST could be

$$\theta = \frac{T - T_\infty}{T_w - T_\infty} \tag{10}$$

here $T_w - T_\infty = \frac{x^F}{b}$

(b) On behalf of arranged heat flux AHF, the wall heat fluctuation is taken to changeable with radial remoteness r(x) beginning the symmetrical axis to the wall of the cylinder and we create the dimensionless hotness by

$$h = \frac{T - T_\infty}{T_w - T_\infty} \tag{11}$$

here $T_w - T_\infty = (\frac{x^H}{K})(\frac{b}{Gr^{\frac{1}{4}}})$, H is the surface heat flux parameter.

The continuity equation could be combined by creating a run function $\psi(x,y)$ as $ur = \frac{\partial r\psi}{\partial y}$, $vr = -\frac{\partial r\psi}{\partial x}$. That fulfills equation (1). Consequently, eqns (2-4) can be written in nonlinear system of PDEs as:

(a) On behalf of AST case

$$(1+s)p''' + sL' + (\theta + d\theta^2)\frac{sin(\alpha)}{\alpha} - (p')^2 + \alpha(cot(\alpha)pp' + \frac{\partial p}{\partial \alpha}p'' - \frac{\partial p'}{\partial \alpha}p') + pp'' = 0 \tag{12}$$

$$(1+\frac{s}{2})L'' - s(2L+p'')p'L + \alpha(cot(\alpha)pL' + \frac{\partial p}{\partial \alpha}L' - \frac{\partial L}{\partial \alpha}p') + pL' = 0 \tag{13}$$

$$\theta'' + Pr(\alpha(\alpha Ec(p'')^2 + cot(\alpha)p\theta' + F\theta' + \frac{\partial p}{\partial \alpha}\theta' - \frac{\partial \theta}{\partial \alpha}p') - Fp'\theta) = 0 \tag{14}$$

Lead to the boundary conditions

$$\text{at } \eta = 0 : p'(0) = G1p''(0), \frac{\partial p(0)}{\partial \alpha} = 0, \theta(0) = 1 + G3\theta'(0), \frac{\partial \theta(0)}{\partial \alpha} = -F + (Gr^{\frac{1}{4}} - FG3)\theta'(0), L(0) = -\lambda f''(0), \frac{\partial L(0)}{\partial \alpha} = G2f''(0)$$

$$as\eta \to \infty : p' = 0, \theta = 0, L = 0, \tag{15}$$

(b) For AHF case

$$h'' + Pr(\alpha(\alpha Ec(p'')^2 + cot(\alpha)ph' + Hh' + \frac{\partial p}{\partial \alpha}h' - \frac{\partial h}{\partial \alpha}p') - Hp'h) = 0 \tag{16}$$

Lead to the limit states

$$\text{at } \eta = 0 : h'(0) = -G4, \frac{\partial h}{\partial \alpha} = Gr^{\frac{1}{4}}h'(0) - \frac{H}{\alpha}h(0)$$

$$as\eta \to \infty : h = 0, \tag{17}$$

Where, $(','',''')$ stand for differential with respect to η, $\alpha = \frac{x}{b}$ represents Dimensionless stream-wise coordinate, $G1 = \frac{aGr^{1/4}}{b}$, $G2 = \lambda(\alpha - b)$, $G3 = \frac{cGr^{1/4}}{b}$ and $G4 = \frac{K}{K+c}$, are velocity, micro rotation and thermals slip parameters correspondingly. $s = \frac{\kappa}{\mu}$, is material parameter, $Gr = \frac{b^3 gN(T_w - T_\infty)}{\nu^2}$ denotes the ratio of the buoyancy forces occur from temperature difference to the viscous force times inertia force to viscous force called as thermal Grashof numbers, $d = \frac{N_t(T_w - T_\infty)}{N}$ is thermal non linear convection parameters. We note that for $d = 0$, the flow

of eq. (13) becomes linear convective micro polar fluid. $Pr = \frac{\rho \nu c_p}{K}$ is prandtl number, $Ec = \frac{\nu^2 Gr^{\frac{3}{4}}}{c_p b^3 x^H} = \frac{\nu^2}{c_p j K(T_w - T_\infty)}$ is Eckert number for AHT and $Ec = \frac{\nu^2 Gr}{c_p b^2 x^F} = \frac{gN}{c_p}$ is Eckert number for AST, F and H stand for power index of terms in non-isothermal surface.

It can be shown that the lower point of the cylinder $\alpha \approx 0$, eq.(12) to eq.(17) reduced to the following non linear system of ordinary differential equations.

(a) For AST case

$$(1+s)p''' + sL' + (\theta + d\theta^2) - (p')^2 + pp'' = 0 \tag{18}$$

$$(1+\frac{s}{2})L'' - s(2L + p'')p'L + pL' = 0 \tag{19}$$

$$\theta'' - PrFp'\theta = 0 \tag{20}$$

Subject to the boundary conditions

$$\text{at } \eta = 0 : p'(0) = G1p''(0), \theta(0) = 1 + G3\theta'(0), L(0) = -\lambda f''(0)$$

$$as\eta \to \infty : p' = 0, \theta = 0, L = 0, \tag{21}$$

(b) For AHF case

$$h'' + Pr(-Hp'h) = 0 \tag{22}$$

Lead to the limit states

$$\text{at } \eta = 0 : h'(0) = -G4$$

$$as\eta \to \infty : h = 0, \tag{23}$$

The important physical quantities of accepting in this problem are the reduced skin friction coefficient C_f,wall couple stress m_w, and the Nusselt number Nu as:

$C_f = \frac{\tau_w}{\rho(u_w)}, Nu = \frac{q_w}{\kappa(T_w - T_\infty)}$,

$$m_w = -(\nu + \frac{\kappa}{2\rho})j(\frac{\partial M}{\partial y})_(y = 0). \tag{24}$$

Where,$\tau_w = (\mu + \kappa)(\frac{\partial u}{\partial y})_(y = 0) + \kappa(M)_0$, $q_w = -K((\frac{\partial T}{\partial y}))_(y = 0)$,

Using the non dimensional variables (9-11) and the boundary conditions (17) the reduced skin friction coefficient C_f, wall couple stress m_w, and the Nusselt number Nu are

$$p''(0) = j\frac{1+s-\lambda}{a^2 \alpha Gr^{\frac{1}{4}} c_f}, -L'(0) = \frac{m_w\sqrt{j}}{\nu^2 \alpha(1+\frac{s}{2})Gr^{\frac{1}{4}}}, Nu\sqrt{j} = -\theta'(0) = -h'(0). \tag{25}$$

3 Numerical Rsult

The numerical solutions of physical constraints are established using the function bvp4c from matlab software which is a fixed difference code that makes real the three- stage Lobatto IIIa formulation. The two stages to be appropriate for the function bvp4c from matlab are:

1. First, Eqs. (12-17) are converted into a system of first-order equations.

2. Secondily, set up a boundary value problem (bvp) and apply the bvp solver in matlab to solve this scheme.

Taking on an appropriate finite value for the ambient field boundary state, that is, $\eta \to \infty$, say $\eta_\infty = 7$ and the step-size is taking in account as $\triangle\eta = 0.01$; and exactness to the fifth decimal place as the degree of convergence. In calculating the BVP using matlab, bvp4c has only three point of views: a function ODEs for calculation of the residual in the boundary states, and a developing solint that gives a guess for a mesh. The order differential equations are controlled exactly as in the Matlab IVP solvers. Further clarification on the process of bvp4c is obtained in the book by Shampine et al.[16].

Let $y(1) = p$, $y(2) = p'$, $y(3) = p''$, $y(4) = L$, $y(5) = L'$, $y(6) = \theta$, $y(7) = \theta'$, $y(8) = \frac{\partial p}{\partial \alpha}$, $y(9) = \frac{\partial L}{\partial \alpha}$, $y(10) = \frac{\partial \theta}{\partial \alpha}$, $y(11) = \frac{\partial p'}{\partial \alpha}$ and
y=[p, p', p'', L, L', θ, θ', $\frac{\partial p}{\partial \alpha}$, $\frac{\partial L}{\partial \alpha}$, $\frac{\partial \theta}{\partial \alpha}$, $\frac{\partial p'}{\partial \alpha}$ $]^T$ gives,

$$\frac{d}{d\eta}\begin{pmatrix} y(1) \\ y(2) \\ y(3) \\ y(4) \\ y(5) \\ y(6) \\ y(7) \\ y(8) \\ y(9) \\ y(11) \end{pmatrix} = \begin{pmatrix} y(2) \\ y(3) \\ (1/(1+s)) * (y(2)*y(2) - (y(1) + \alpha * cot(\alpha) * y(1)) * y(3) + \\ \alpha * (y(11)*y(2) - y(8)*y(3)) - s*y(5) - (y(6) + d*y(6)*y(6)) * \frac{sin(\alpha)}{\alpha}) \\ y(5) \\ (1/(1+0.5*s)) * (y(4)*y(2) + s*(2*y(4)+y(3)) - y(1)*y(5) \\ -\alpha * cot(\alpha) * y(1) * y(5) - \alpha * (y(10)*y(5) - y(11)*y(2))) \\ y(7) \\ -Pr * (y(1)*y(7) + \alpha * cot(\alpha) * y(1) * y(7) + \\ \alpha * (y(8)*y(7) - y(10)*y(2) - \alpha * Ec * y(3) * y(3)) - F * y(6) * y(2)) \\ y(8) \\ y(9) \\ y(10) \\ y(11) \end{pmatrix} \tag{26}$$

4 Outcome with Discussion

In this subsection, we present the effect obtained by developing numerical technique for the problem under kindness for each flow areas.

4.1 Velocity and micro-rotation Profiles

The impact of H, F, d, G1, j, α, Ec, λ and s on non dimension velocities $p'(\eta)$, and $L(\eta)$ are shown in Fig. 2-Fig. 11. Fig. 2 and Fig. 6, show that enlarge values of H and j increase the kinematic viscosity of the fluid which enhance the opposition to flow the fluid that cause decrease the flow of the fluid $p'(\eta)$ within the boundary layer.

Fig. 3,Fig. 4and Fig. 5 reveal that increase values of F, d and G1 decrease the viscosity of the fluid which increase the flow of the fluid $p'(\eta)$ near the surface of the cylinder and decline as far from the wall of cylinder. Moreover, the velocity profile exhibits enhancing behavior within the boundary layer of it for improving values of Ec and α as seen in Fig. 7and Fig. 8.

Feature of dimensionless stream-wise coordinate α, material s, and angular λ constraints on $L(\eta)$ are illustrated in Fig. 9, Fig. 10, and Fig. 11. The improving α, s and λ resulted in a decrementing, an incrementing and a decrementing behavior of $L(\eta)$. It is markable that the curves of $L(\eta)$ are constant for lower values η and then begin to enhance for material

constraint s and to go down for dimensionless stream-wise coordinate α and angular λ constraints.

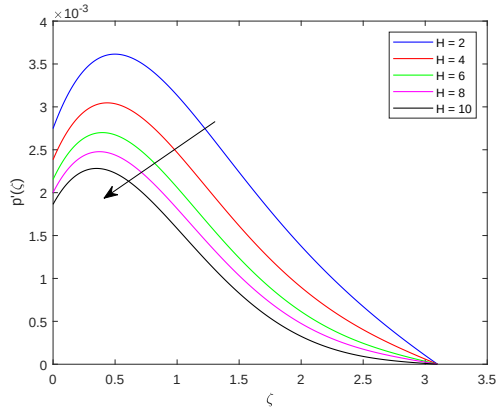

Fig. 2 – Impact of H on $p'(\eta)$ profile when$Gr = \lambda = d = 0.1, G1 = 0.7, Ec = s = 0.2, G2 = j = 0.5, Pr = 7, \alpha = 30$

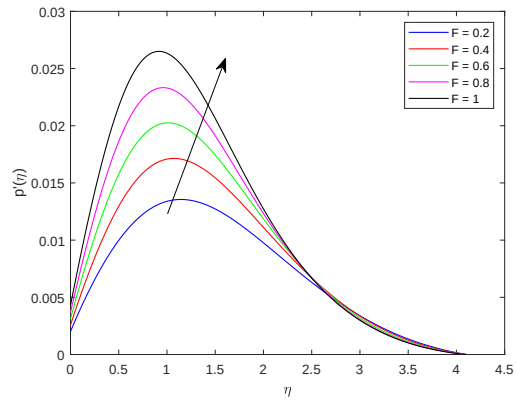

Fig. 3 – Result of F on $p'(\eta)$ for Gr = 0.7, Ec = 0.5, s = 0.1

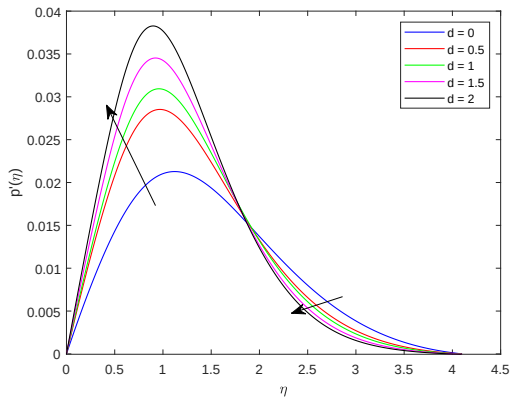

Fig. 4 – Result of d on $p'(\eta)$ for Gr = 0.6, G1 = 0

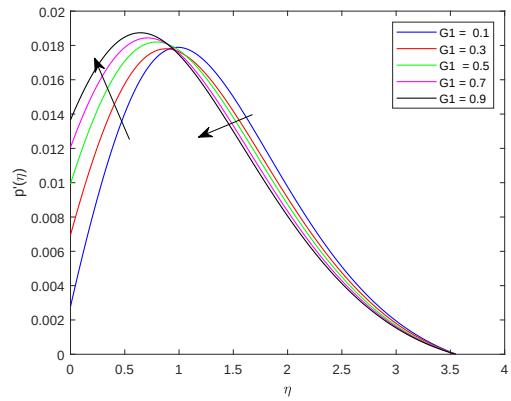

Fig. 5 – Result of G1 on $p'(\eta)$ for Gr = 0.6, s = 0.12

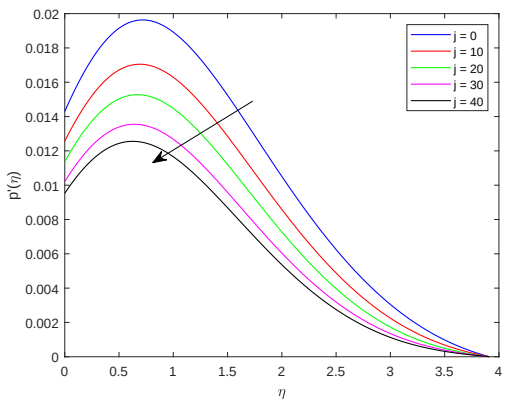

Fig. 6 – Impact of j on $p'(\eta)$ when s = 0.35, G1 = 1

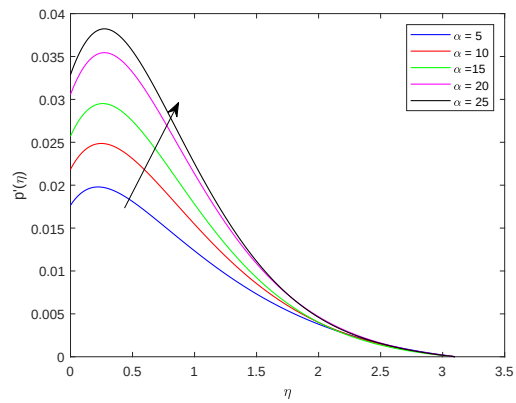

Fig. 7 – Impact of α on $p'(\eta)$ when Gr = 10, G1 = 0.8, s = 0.1, d = 11

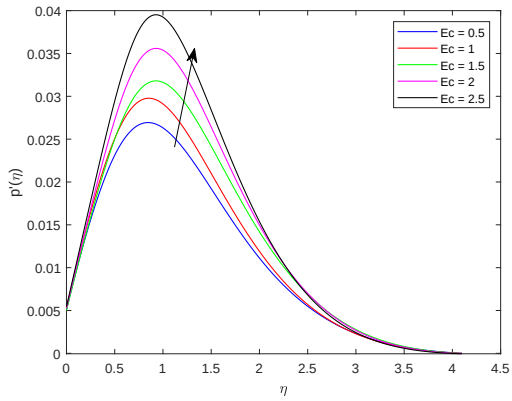

Fig. 8 – Result of Ec on $p'(\eta)$) profile for Gr = 0.63, G1 = 0.11, F = 0.6, G1 = 0.5, λ = 0.7, d = j= 0.1

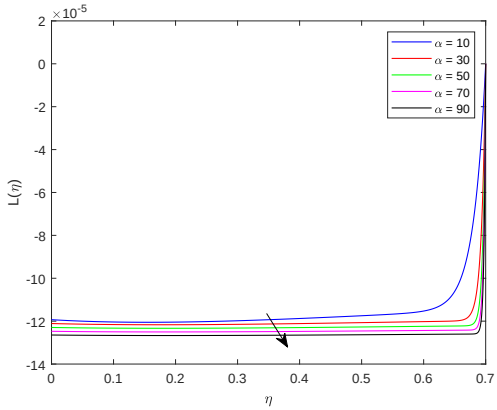

Fig. 9 – Result of α on $L(\eta)$ for Gr = 12, s = 0.9

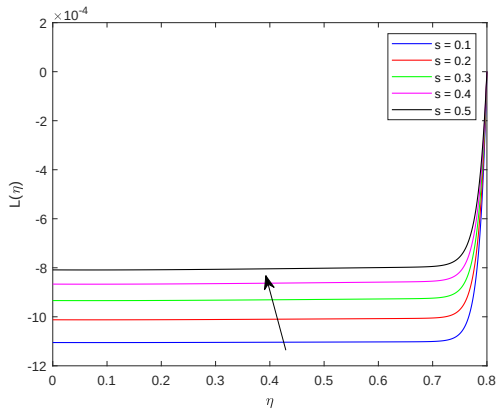

Fig. 10 – Result of s on $L(\eta)$ for Gr = 4, λ = 0.3

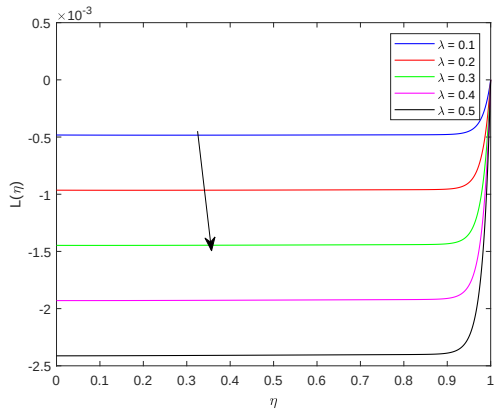

Fig. 11 – Impact of λ on $L(\eta)$ when Gr = 3

4.2 Temperature Profiles

The significance of F, H, Ec, α, Gr, s, G3, G4, d on temperatures, $\theta(\eta), h(\eta)$ are elucidated in Fig. 12-Fig. 25. Fig. 12- Fig. 13 demonstrate that increase of surface temperature and heat flux parameters (F,H), enhance the thermal conductivity of involved material which result augment in hotness profiles θ, h. However, the temperature distributions exhibit the declining performance for enlarge Ec and thermal non linear convection parameter d as shown in Fig. 14-Fig. 17. These behaviors are happened due to reduction of thermal conductivity of the fluid which is lower for larger Ec and d. The smaller thermal conduction relates to lower temperature. The kinetic energy is reduced for greater Ec because of the fluid turn out to be cooler. This occurrence resulted in the creation of lower temperature.

Fig. 18- Fig. 19 address that boost of micro inertia per unit mass j, enhance thermal conductivity of the fluid near the wall of cylinder and decline it near far from the surface of cylinder which result the increment of temperature distributions at the surface and decrement of temperature profiles at far from the surface of cylinder. Fig. 20 and Fig. 21 illustrate that improve Gr and material parameter s,decline the viscosity of the fluid which relate to upsurge temperature profile case i.e in AHT and the temperature distribution, in the case of AHT shows the increasing behavior for growth values of thermal slip parameter in the case of AHT G4 as revealed in Fig. 23. This increasing behavior of temperature distribution is caused due to

increment of thermal conductivity of the fluid which enhance kinetic energy for larger G4 as the fluid becomes hotter. Here the phenomenon caused in the creation of higher hotness of the flow.

Fig. 22 explain that enhance of thermal slip in the case of AST G3, go down the viscosity of the fluid which decline thermal diffusion within the boundary layer that associate through decrease in temperature. It observed that α exhibits opposite effect on temperature in case of AST and AHF as seen in Fig. 24 and Fig. 25. Fig. 26-Fig. 29 elucidate the grid-independence test. From these figures, it is seen that for the digit of points larger than apposite mesh digit of points, the precision is not affected.

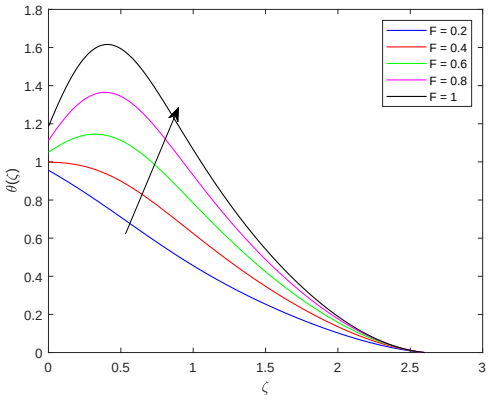

Fig. 12 – Impact of F on $\theta(\eta)$ profile when $Gr = 0.7, \lambda = d = G1 = 0.6, Ec = s = 0.2, G2 = j = 0.5, Pr = 7, \alpha = 30$ for AST

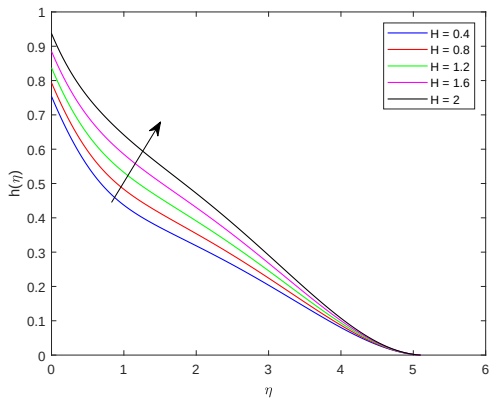

Fig. 13 – Result of H on $h(\eta)$ for G1 = Ec = 1, Gr = 0.5 for AHF

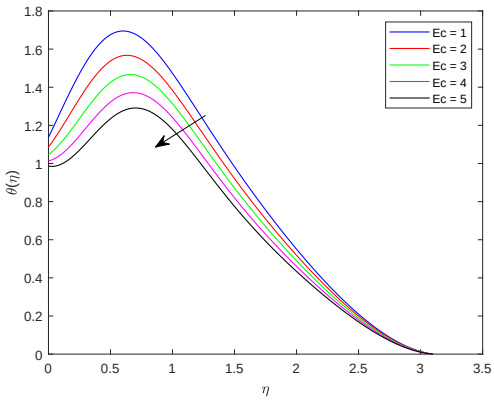

Fig. 14 – Impact of Ec on $\theta(\eta)$ profile when Gr = 0.1 for AST

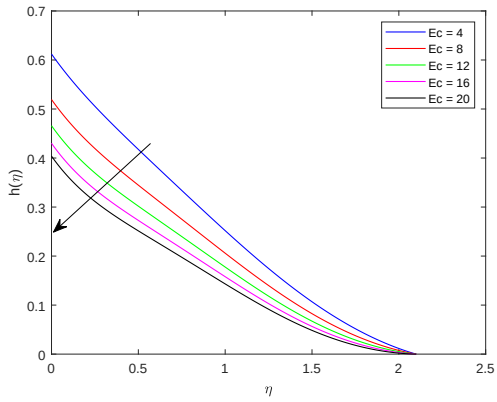

Fig. 15 – Result of Ec on $h(\eta)$ for H = 1, j = 0.1 for AHF

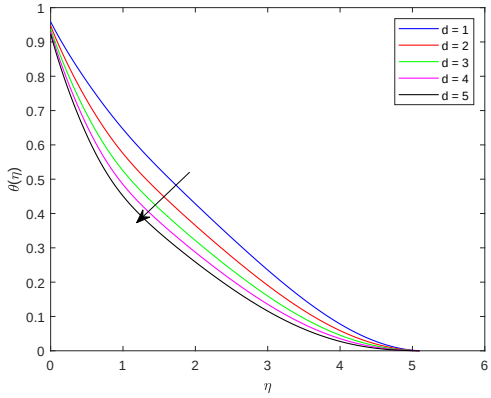

Fig. 16 – Result of d on $\theta(\eta)$ for Gr = 0.1, F = 0.1 for AST

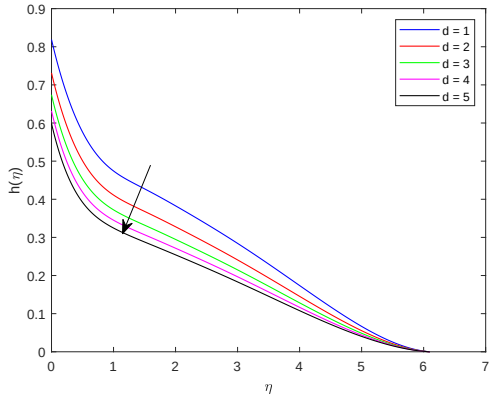

Fig. 17 – Impact of d on $h(\eta)$ profile when H = 1, Ec = 0.5 for AHF

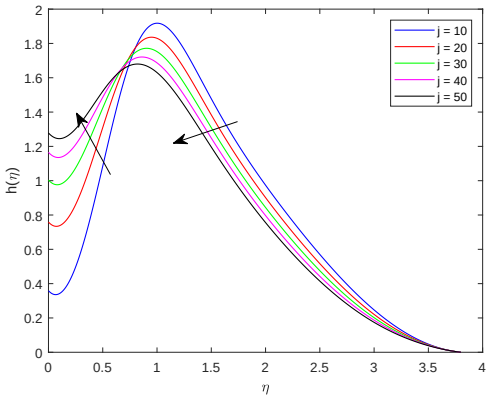

Fig. 18 – Impact of j on $h(\eta)$ profile when H= 1, Ec = Gr = 4, d = 0.1 for AHF

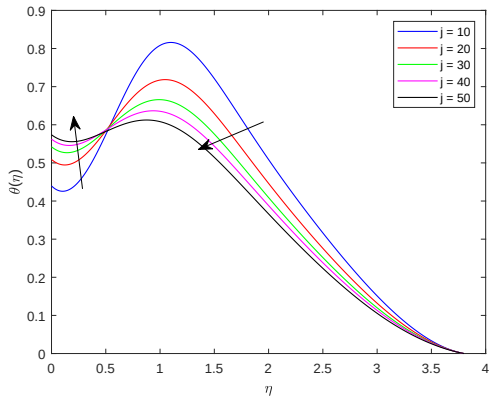

Fig. 19 – Result of j on $\theta(\eta)$ for G1 = Ec = 3, s = 0.1, G3 = 2 for AST

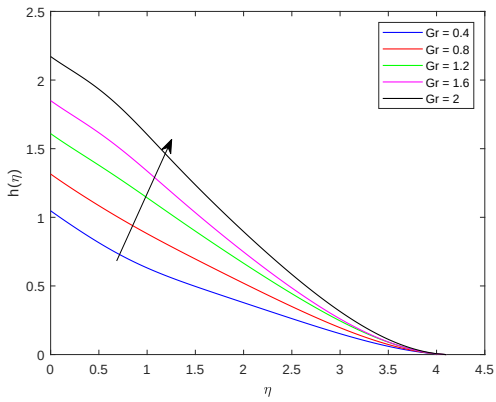

Fig. 20 – Result of Gr on $h(\eta)$ for H = 2, Ec = 0.1 for AHF

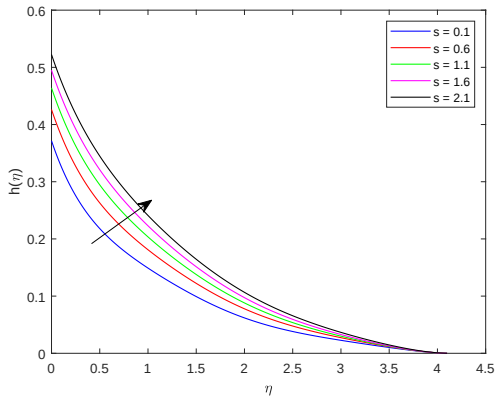

Fig. 21 – Impact of s on $h(\eta)$ profile when d = Gr = G1 = j = 0.1, G2 = G4 = 0.5, Ec = 10, $\lambda = 0.7$for AHF

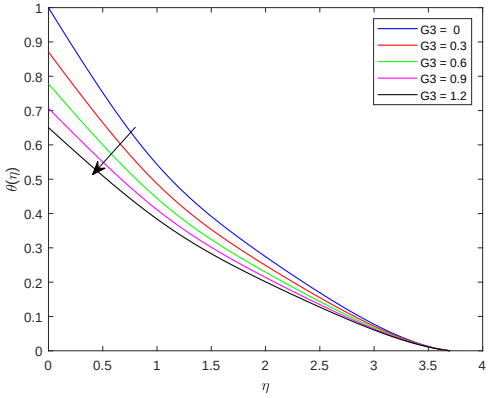

Fig. 22 – Impact of G3 on $\theta(\eta)$ profile when Gr = G1 = F = d = 0.1, j = 0.5, Ec = 0.12 for AST

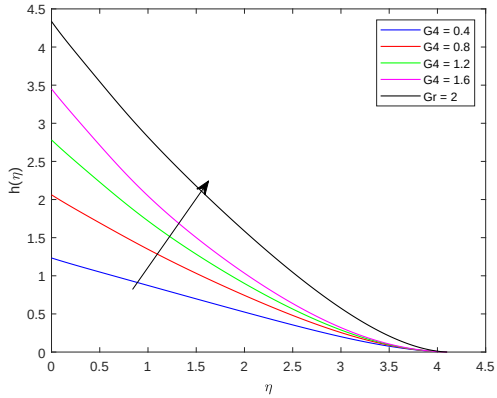

Fig. 23 – Impact of G4 on $h(\eta)$ profile when H = 2, Ec = 0.1, for AHF

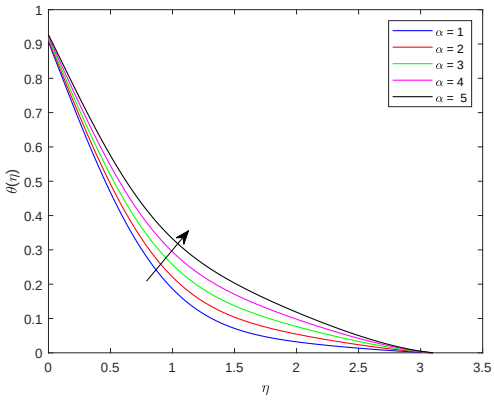

Fig. 24 – Result of α on $\theta(\eta)$ for Gr = 0.5 for AST

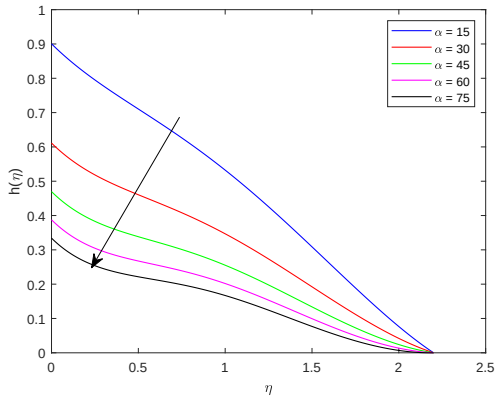

Fig. 25 – Impact of α on $h(\eta)$ profile when H= 5, Gr = 1, Ec = 8 for AHF

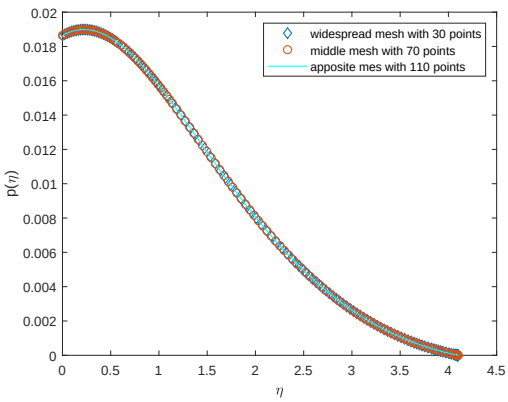

Fig. 26 – Grid-independence test on $p(\eta)$ when G1 = 6, Gr = 2

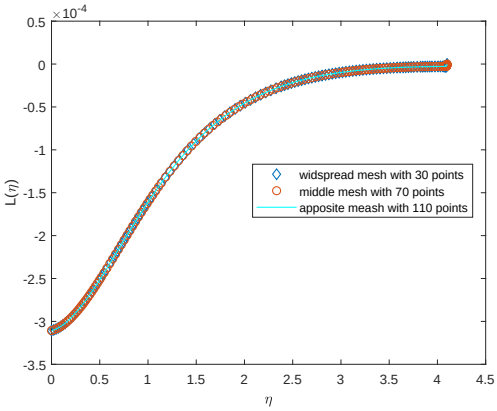

Fig. 27 – Graph Grid-independence test on $L(\eta)$ when G1 = 6, Gr = 2

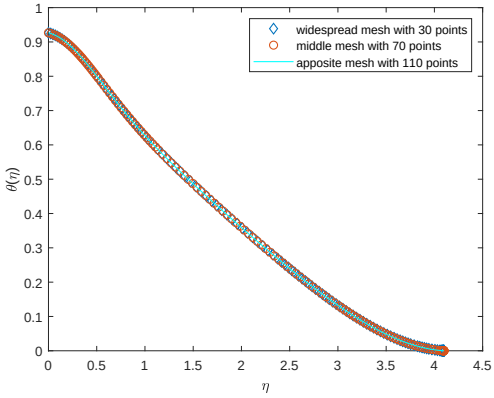

Fig. 28 – Grid-independence test on $\theta(\eta)$ when G1 = 6, G3 = 1, F = 0.1, Gr = 2 for AST

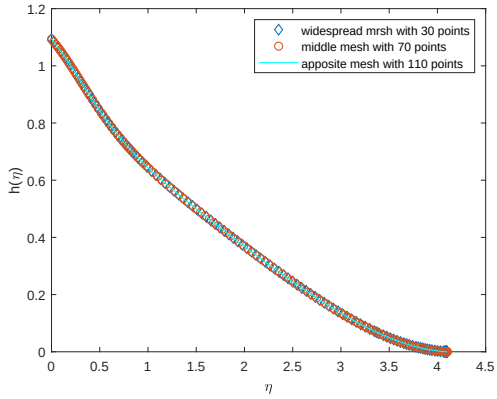

Fig. 29 – Grid-independence test on $h(\eta)$ when G1 = 6, G4 = 0.4, H = 1, Gr = 2 for AHF

The presentation of grid independence test is revealed in the Table 1, to maintain the point of exactness called as grid convergence test. It initiated by the widespread mesh with 30 number of points. By adding 40 and 80 number of points to widespread, we have the middle mesh ,70 and the apposite mesh, 110 points of truthfulness for velocity, and temperature gradient values. For the number of spots larger than apposite mesh number of spots, the correctness is not affected.

Table 1 – Grid-independence test for velocity gradient $p''(\eta) and \theta'(\eta)$ when $Gr = 2, G1 = 6, F = \lambda = 0.1, Ec = d = 0.2, Pr = 7, G2 = j = 0.5, \alpha = 30$.

	widespread mesh, 30		middle mesh, 70		apposite mesh, 110	
s	$p''(\eta)$	-$\theta'(\eta)$	$p''(\eta)$	-$\theta'(\eta)$	$p''(\eta)$	-$\theta'(\eta)$
0	0.0028	0.2078	0.0028	0.2078	0.0028	0.2078
1	0.0025	0.1539	0.0025	0.1539	0.0025	0.1539
2	0.0023	0.1311	0.0023	0.1311	0.0023	0.1311
3	0.0020	0.1195	0.0020	0.1195	0.0020	0.1195
4	0.0018	0.1130	0.0018	0.1130	0.0018	0.1130

Table 2 drawn to put side by side the exactness of the technique used association with earlier presented data feasible in the literatures have been made. From Table 2 it can be seen that the numerical values of the Nusselt number -$\theta'(0)$ in current study for various values of s and α when λ=0.5, Pr = 0.7 is in an excellent agreement with the pervious outcomes of reported studies by[17] and [13]. The results indicate that the numerical used in the information is truthful and highly accurate.

Table 2 – Comparison of Nusselt number -$\theta'(0)$ when $\lambda = 0.5$, Pr = 0.7 for different values of s and α with previously published result.

		present result	[12]	[13]	[17]
s	α	-$\theta'(0)$	-$\theta'(0)$	-$\theta'(0)$	-$\theta'(0)$
0.0	0.0	0.4576	0.4576	0.4577	0.4576
0.5		0.4336	0.4336	0.4334	0.4336
1.0		0.4163	0.4165	0.4166	0.4166
1.5		0.4035	0.4037	0.4040	0.4035
2.0		0.3931	0.3931	0.3932	0.3930
0.0	10	0.4564	0.4561	0.4560	0.4565
	20	0.4536	0.4535	0.4534	0.4533
	30	0.4481	0.4481	0.4486	0.4480
	40	0.4404	0.4406	0.4406	0.4405
	50	0.4309	0.4309	0.4309	0.4308
	60	0.4188	0.4189	0.4188	0.4189
	70	0.4048	0.4048		0.4046
	80	0.3873	0.3878		0.3879
	90	0.3687	0.3687		0.3684

Table 3 indicate that increase in values of Ec and d, cause increasing in both the skin friction coefficient $p''(0)$, and Nusselt number $-\theta'(0)$. These result happen because of reducing thermal conductivity of the fluid which cause improve the diffusion of momentum and temperature that associate through increment of these physical quantities. Since gravity of the earth increase because of buoyancy force which increases the density of fluid results the skin friction coefficient $p''(0)$, and Nusselt number $-\theta'(0)$ growth.

Table 3 – The computed values of skin friction coefficient p"(0), Nusselt number -$\theta'(0)$ when Gr = 2, G1 = 0.6, G3 = 0.3, λ = G2 = 0.1, F = s= 0.2, j = 0.5, α= 30, Pr = 7 for different values of Ec and d

Ec	d	$p''(0)$	-$\theta'(0)$
0	0.2	0.0138	0.0209
0.5	0.2	0.0140	0.0560
1	0.2	0.0142	0.0938
1.5	0.2	0.0144	0.1344
2	0.2	0.0146	0.1785
0.5	0.1	0.0132	0.0217
	0.3	0.0144	0.0334
	0.5	0.0156	0.0440

5 Conclusions

This study considers the consequences of governing dimensionless physical quantities such as the surface temperature and heat flux parameters, thermal non-linear convection, Eckert

number and multiple slip states on a micro-polar fluid past a non isothermal cylinder. Results of governing boundaries are presented by using figures and tables. The main results are:

1. Enlarging the values of surface temperature and heat flux parameters (F, H) agree to enhance thermal diffusion that improve temperature distributions $\theta(\eta), h(\eta)$.

2. The surface temperature and heat flux distributions(θ, h) within the boundary can be reduced by the enhance in values of Eckert number and non-linear convection parameter which decrease the thermal conductivity (diffusion)of the fluid.

3. The existence of dimensionless stream-wise coordinate agree to upsurge in temperature distribution θ and velocity profile $p'(\eta)$ within boundary layer whereas it allows to decline in heat flux distribution.

4. An enhancement in the values of G4,s result in increment of the heat flux within boundary layer.

5. Boosting microinertia per unit j tolerate to enhance thermal conductivity of the fluid near the wall of cylinder and upsurge viscosity of the fluid near far the surface of cylinder which result the increment of temperature distributions at the surface and decrement of temperature profiles at far the surface of cylinder as well as declining the velocity profile.

Availability of data and Materials
Data distribution not valid to this paper as no data sets were analyzed throughout the current study.
Conflict of interest: Authors have no conflict of interest relevant to this article.

References

[1] Pabst W.(2005). Micropolar Materials, ceramics-Silikaty, 49(3),170-180.

[2] Calimelet E.C., Majumdar D.R.(1998).Flow of a micropolar fluid through a cilcular cylinder subject Longtudinal and Torsional oscilation, Mathl.Comput. Modelling vol. 27, No 8, pp 69-78.

[3] Reena, Rena U.S. (2009), Effect of Dust particles on Rotating Micropolar fluid Heated From below saturating a porous medium, Applications and Applied Mathematics,An International Journal, vol.4 No 1 pp 189-217.

[4] Gajjela N., Matta A.,Kaladhar K.(2017), Chemica reaction, Hall and ion currents on Magnetized micropolar flow through co-rotating cylinders, AIP Advance, 7,115201.

[5] Machireddy G.R.(2013), Chemically reaction Species and radition effects on MHd convective flow past a moving vertical cylinder, AcnShems Engineering Jouernal, 4,879-888.

[6] Shah Z., B. McCash L., Dawar A., Bonyah E.(2020). Entropy Optimi zation in Darcy-Farchheimer MHD flow of water based copper and Siliver nanofluids with Joule heating and viscous dissipation Effects, AIP Advence,10,065137.

[7] Reddy M.G., Ferdous M.(2020). Species and thermal radiation on micropolar hydromagnetic dusty flow across a paraboloid revolution, Journal of thermal Analysis and Calorimetry.

[8] Reddy M.G., Vijayakumar P., Kumar K.G., Sherzad S.A.(2020). Zero massflux and CattoneoChristov heat flux through a prantl nonNewtonian nanofluid in Darcy- Forchheimer porous space, Heat transfer, 1-14.

[9] Sherzad S.A., Reddy M.G., Rauf A., Abbas Z.(2020).Biconvection of Maxwell Nanofluid under the Influence of double diffusive Cattaneochristov theories over isolated rotating disk, Physica Scripta, 95,045207,17.

[10] Salleh M.Z., Nazar R.,Pop I.(2010), Mixed convection boundary layer flow from a solid sphere with Newtonian heating in a micropolarfluid, S cholary Research Exchange, vol.2010, 736039.

[11] Wubshet I., Shanker B.(2014), MHD boundary layer flow and heat transfer of a nanofluid over Non- isothermal stretching sheet, Journal of Heat Transfer,vol. 136,051701-9.

[12] Wubshet I., Chaluma Z.(2020). Non-linear Free Convection Flow of Micro-polar Nanofluid over a Cylinder, Journal of Heat Transfer, 22038.

[13] Wubshet I., Chaluma Z.(2019). Non-linear convection flow of micropolar nanofluid past an isothermal sphere, Journal of Physics Communications 3, 115017.

[14] Wubshet I., Chaluma Z.(2020). MHD Non-Linear Natural Convection Flow Of Micropolar Nano-Fluid past a Non-Isothermal Rotating Disk, Journal of Heat Transfer,50, 21894.

[15] Amanulla CH , Abderrahim W., Zoubair B., M.S. Reddy M.S., Nagendra N.(2018). Numerical investigations on magnetic field modeling Carreau non-Newtonian fluid flow past an isothermal sphere, Journal of the Brazilian Society of Mechanical Science and Engineering 40:462.

[16] Shampine L.F., Glandwell I., Thomson S.(2003). Solving ODEs with Matlab, Cambridge, New York, USA.

[17] Nazar R., Amin N., Grosan T .,,Pop I.(2002). Free Convection boundary layer on an isothermal sphere in a micropolar fluid, Int. comm. Heat transfer vol.29, No.3, pp. 377-386.